

# EXPERIMENTAL RESEARCH PROGRESS TOWARD THE VASIMR ENGINE

**Jared P. Squire<sup>1</sup>, Franklin R. Chang Díaz<sup>2</sup>, Verlin T. Jacobson<sup>1</sup>, Tim W. Glover<sup>3</sup> F. Wally Baity<sup>4</sup>, Richard H. Goulding<sup>4</sup>, Roger Bentson<sup>5</sup>, Edgar A. Bering, III<sup>6</sup>, and Kristy A. Stokke<sup>7</sup>**

<sup>1</sup>Muñiz Engineering, Inc., Advanced Space Propulsion Laboratory, NASA Johnson Space Center, Houston, Texas, 77059 USA

<sup>2</sup>Advanced Space Propulsion Laboratory, NASA Johnson Space Center, Houston, Texas, USA

<sup>3</sup>Rice University, Advanced Space Propulsion Laboratory, Houston, Texas, USA

<sup>4</sup>Oak Ridge National Laboratory, Oak Ridge, Tennessee, USA

<sup>5</sup>University of Texas at Austin, Austin, Texas, USA

<sup>6</sup>University of Houston, Houston, Texas, USA

<sup>7</sup>Massachusetts Institute of Technology, Cambridge, Massachusetts, USA

## ABSTRACT

The Advanced Space Propulsion Laboratory (ASPL) of NASA's Johnson Space Center is performing research on a Variable Specific Impulse MagnetoPlasma Rocket (VASIMR), a high power, radio frequency (RF) driven magnetoplasma rocket. The experimental research focuses on three major areas: helicon plasma production, ion cyclotron resonant frequency (ICRF) acceleration and plasma expansion in a magnetic nozzle, with this paper presenting recent experimental results regarding the first two. A flexible four-magnet system, with a 1.3 Tesla maximum magnetic field strength, is used to study axial magnetic field profile shape effects. Up to 3 kW of 25 MHz power is used for helicon plasma source development, primarily in helium for this work. A 3 MHz RF transmitter is used at powers up to 6 kW for ICRF experiments. Optimization studies have been performed with the magnetic field axial profile shape, gas flow rate, and antenna geometry. Gas efficiencies of near 100% are achieved with strategic gas baffling. Power efficiency scales favorably with plasma diameter in the 5 to 7 cm range. We measure supersonic flow velocities ( $>$  ion sound speed) in the exhaust section. A strong coupling between the neutral gas pressure and the plasma discharge is observed in the source. Axial profiles of heating on the helicon gas tube wall are peaked under the antenna and correlate with light emission profiles. Initial ICRF experiments have been performed, using a helium helicon discharge as a target. Up to 6 kW of power has been applied using a simple unoptimized antenna array at both the fundamental and second harmonic of the cyclotron resonance. Results with the fundamental resonance are presented. Future plans for ICRF experiments are discussed.

## INTRODUCTION

Most electric propulsion concepts rely on electrostatic fields to accelerate plasma ions to produce thrust. These concepts require electrodes and materials that are in contact with the plasma so are subject to erosion, which limits the thruster's lifetime. The electrostatic field configuration may also limit the achievable ion velocity, especially when combined with high ion flux density. These challenges become increasingly difficult when a deep space mission requires high power ( $>100$  kW), high ion velocity ( $>60$  km/s) and very long lifetimes ( $> 4$  years). One solution to these problems is to drive a thruster with radio frequency (RF) power, thus eliminating the need for electrodes and thus enabling dense energetic plasmas flows. Furthermore, the thruster could use a magnetic field to control the flow of the plasma and prevent it from eroding any

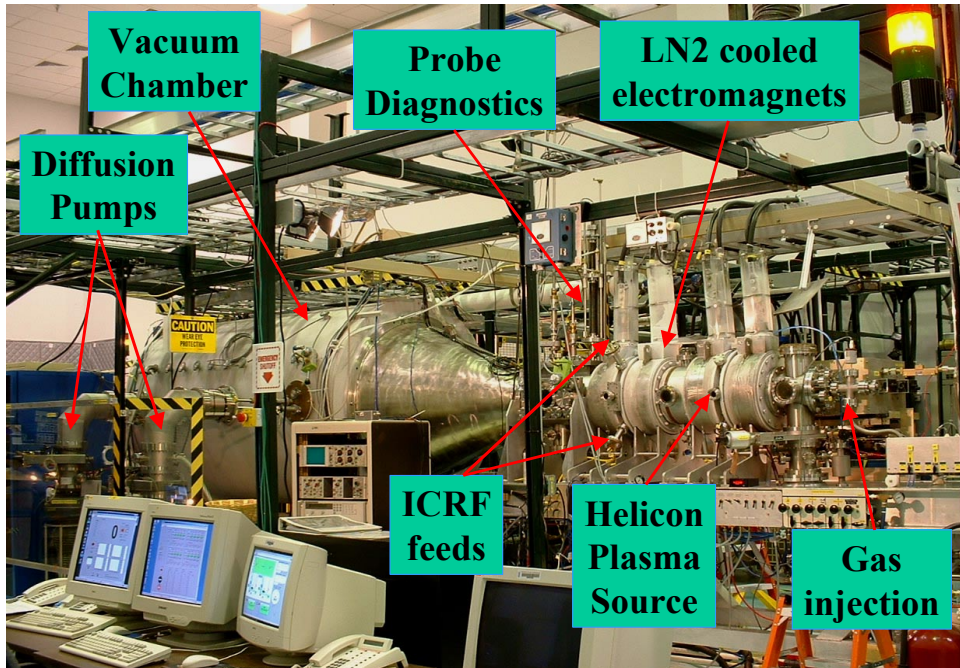


FIGURE 1 Recent photograph of the VX-10 laboratory system.

surrounding materials. The Variable Specific Impulse Magnetoplasma Rocket (VASIMR) concepts incorporates these features.<sup>1</sup>

The VASIMR is a high power, radio frequency (RF) driven magnetoplasma rocket, capable of very high exhaust velocities, > 100 km/s. The Advanced Space Propulsion Laboratory (ASPL) of NASA's Johnson Space Center leads a research team involving industry, academia and government facilities that is pursuing the development of this concept in the United States. The ASPL's experimental research focuses on three major areas: helicon<sup>2,3</sup> plasma production, ion cyclotron resonant frequency (ICRF) acceleration and plasma expansion in a magnetic nozzle. The present VASIMR experiment (VX-10) performs experimental research that demonstrates the thruster concept at a total RF power on the order of 10 kW.<sup>4</sup> This paper describes the experiment and recent results.

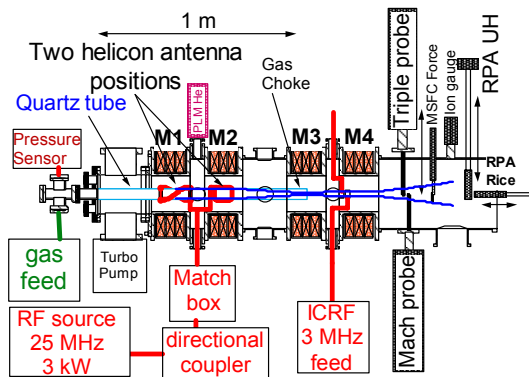


FIGURE 2 VX-10 schematic for two helicon configurations.

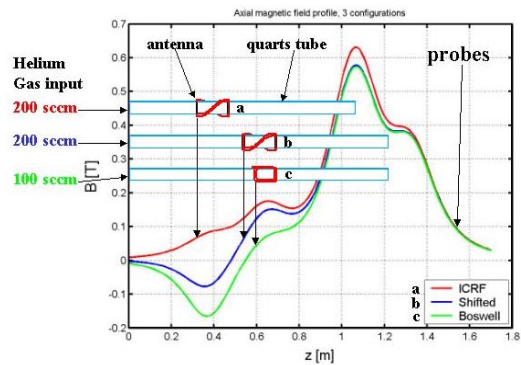


FIGURE 3 Axial magnetic field profiles with three helicon configurations: a (ICRF), b (Shifted) and c (Boswell).

## THE VX-10 EXPERIMENT

Figure 1 contains a photograph of the laboratory system. The configuration schematic for the experimental data presented here is shown in Figure 2.

### The Device

The magnetic system consists of 4 liquid nitrogen cooled electromagnets integrated into a stainless steel vacuum chamber. The magnet coils are designated M1, M2, M3, and M4 starting at the most upstream end. The magnet spacing and independent electrical DC current regulation tailor the axial magnetic field profile. Typically the magnetic field profile provides a low magnetic field strength ( $< 0.2$  tesla) for the helicon plasma source and a high magnetic mirror (up to 1.3 tesla) downstream from the helicon source. Figure 3 shows typical magnetic field profiles.

Neutral gas flow is regulated (10 – 500 sccm) through a port on axis that opens into a quartz tube that is sealed against the inside of the device's end flange cover. The gas flows through the quartz tube, passing through the helicon antenna, into the main vacuum chamber. Recently a gas choke has been installed near the end of the quartz tube at the maximum of the applied magnetic field to reduce the gas flow rate required for optimum discharge conditions. The quartz tube ends before the ICRF antenna. The main vacuum chamber opens into a 4 m<sup>3</sup> chamber that is pumped with two diffusion pumps and one cryopump. The total pumping rate for hydrogen is about 6000 liters/second. The chamber background pressure is kept in the low 10<sup>-4</sup> torr range during a plasma pulse,  $< 3$  second as shown in Figure 4. The addition of the gas choke has reduced this background pressure by more than a factor of two.

Radio frequency (RF) power for the helicon is available at 25 MHz with 3 kW of power. The helicon antenna is water-cooled and resides inside the vacuum chamber. We present data taken

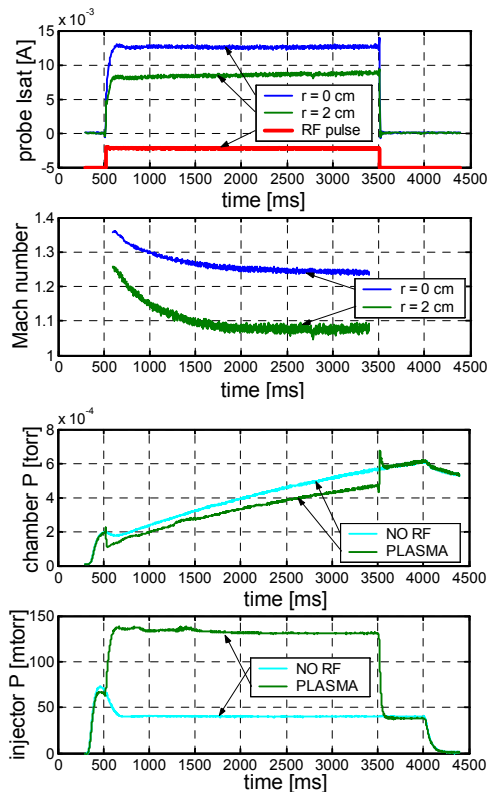


**Figure 4** Temporal behavior of a helicon plasma discharge, without the gas choke.

using a half-turn helical antenna that is 0.15 m in length, which was the plasma source for ICRF experiments. More recently, we have converted to experiments using a Boswell type double saddle antenna, 0.1 m in length. Impedance matching is accomplished using vacuum variable capacitors and power is measured in the 50 Ohm matched section with a directional coupler.

ICRF experiments are performed at a frequency of 3.0 MHz. A transmitter, power splitter and matching network can deliver power at over 40 kW, steady state. The RF power drives a water cooled phased dual half-turn antenna array. The power splitter imposes a 90 degree phase shift to the two array elements, while the feeds are rotated 90 degrees from each other. We phase the array corresponding to either  $m = +1$  or  $-1$  modes by reversing the 50 Ohm power feeds.

### Diagnostics

Reciprocating Langmuir and Mach probes are the primary plasma diagnostics for characterizing the flow out of the exhaust. Together the two probes measure electron

temperature and density profiles with a Mach number. This provides the total plasma flux (ion rate) and flow velocity. Both probes are located just downstream of the last magnet coil. The Langmuir probe has four cylindrical tips that are biased as a triple probe, with an extra tip for measuring floating potential. The Mach probe<sup>5</sup> has two tungsten cylindrical tips biased in ion saturation, one upstream and one downstream of a boron nitride separator. The Mach number is calculated as the average of two models<sup>5,6</sup> with an estimated accuracy of  $\pm 30\%$ .

A microwave density interferometer has been recently installed and provides an electron density calibration for the probe profiles. Also, an electrically floating plate can be put in the plasma exhaust for measuring force and heat flux.<sup>7</sup>

We present data from the probe diagnostics that are profile-averaged quantities as defined by,

$$\langle x \rangle = \frac{1}{\int I_{sat} r dr} \cdot \int x I_{sat} r dr \quad (1)$$

where  $I_{sat}$  is ion saturation current measured on the probe. This weights the averaged quantity to a majority of the ion flux. An important quantity is the total plasma flux or ion rate ( $\Gamma_{plasma}$ ) flowing out of the source. We calculate this using the formula,

$$\Gamma_{plasma} = 2\pi \int n_e M C_s r dr. \quad (2)$$

The plasma Mach number is represented by  $M$  and  $C_s = \sqrt{T_e/m_i}$  is the ion sound speed. The electron density and temperature are  $n_e$  and  $T_e$ , respectively, and  $m_i$  is the ion mass. We note that the product  $n_e C_s$  is relatively insensitive to the electron temperature, so errors in  $T_e$  do not have a significant impact on the  $\Gamma_{plasma}$  measurement. Recent calibration against the density interferometer shows that the probes under estimate the density by a factor of 1.4, so we correct the probe measured density, and consequently the flux, by this factor.

The experiment's primary ion diagnostics are Retarding Potential Analyzers (RPA). We have two designs installed that show good agreement. One RPA is mounted on a long shaft that allows it to scan axial locations from the ICRF antennas to a meter downstream.<sup>8</sup> The RPAs use four biased grids to analyze the ion energy. The axial scanning RPA has a collimator feature, shown in Figure 5, that enables sensitive measurements of ion pitch angle distribution effects. With this feature, only ions with a pitch angle of less than approximately 0.6 degrees are detected.

Figure 6 illustrates the effect of increases in parallel and perpendicular energy on the ion current that passes through the collimator. The horizontal arrow indicates an increase in ion parallel velocity due to acceleration from an increase in plasma potential. The consequent reduction in pitch angle brings the

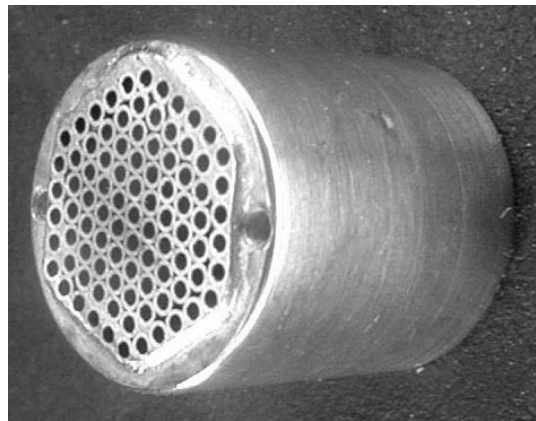


**Figure 5** Collimator for retarding potential analyzer. Individual tubes are 2 cm in length, 0.086 cm in diameter, stainless steel.

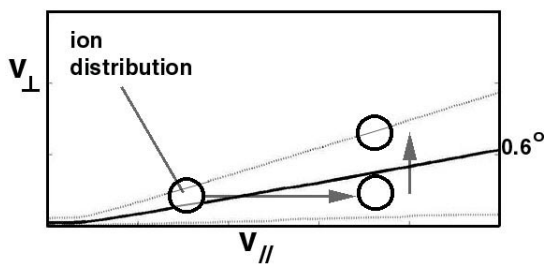


**Figure 6** Simplified ion velocity superimposed on a contour plot of the collimator's transmission function.

distribution into a region of higher collimator transmission, and the ion current increases. The vertical arrow indicates an increase in perpendicular velocity accompanying the increase in parallel velocity. This perpendicular heating raises the pitch angle of the ions and moves the distribution into a region of lower collimator transmission, causing the ion current to drop.

We measure visible light emission axial profiles from the plasma using optics on a sliding seal that couples light out through an optical fiber to a photo diode. The optics views the discharge perpendicular to the axis and can translate the entire length of the helicon section. The temperature increase on the quartz tube during a plasma pulse is measured using thermocouples attached at 10 locations along the tube, thus determining a power density (W/m) profile. The quartz tube absorbs UV and resonance radiation from neutral atoms leading to the temperature rise combined with that attributed to particle flux to the quartz.

Neutral pressures in the system are measured with a magnetically shielded ion gauge mounted in the exhaust region and a baratron mounted to flange open to the upstream end of the quartz tube, as shown in Figure 2. A pitot tube with its opening near the quartz tube inside wall on a sliding seal, not shown, measures the neutral pressure axial profile.

### **HELICON PLASMA SOURCE**

The helicon experiments primarily focus on developing a plasma source to produce a dense target for ICRF experiments. We used helium gas initially, for safety reasons, and have expanded to hydrogen, deuterium, nitrogen, argon, xenon. As others have observed,<sup>9,10,11</sup> generally we find that the helicon source is most efficient at plasma production when the RF frequency ( $\omega_{RF}$ ) is near the lower hybrid frequency ( $\omega_{LH}$ ), for conditions under the antenna, as defined by the following equation,<sup>12</sup>

$$1/\omega_{LH}^2 = 1/\omega_{ce}\omega_{ci} + 1/(\omega_{pi}^2 + \omega_{ci}^2) \quad (3)$$

where  $\omega_{ce}$  and  $\omega_{ci}$  are the electron and ion cyclotron frequencies, and  $\omega_{pi}$  is the ion plasma frequency.

Experiment configurations are explored by optimizing the gas efficiency,  $\eta_{gas} \equiv \Gamma_{plasma}/\Gamma_{gas}$ , where  $\Gamma_{gas}$  is the input gas flow rate. The following sections describe results from these optimized discharges and parameter scans near the optimum. The effects and benefits of having a high magnetic field downstream of the helicon source have been reported elsewhere.<sup>13</sup> Most of the data presented are from helium discharges, unless otherwise noted. Deuterium discharges demonstrate very similar characteristics.

#### **Developing a more compact helicon design**

Much of our earlier work was with a relatively flat magnetic field profile in the helicon section with the antenna located at the upstream end of the device, under M1. We found, however, that magnetic profile shaping in the helicon section, operating M1 and M2 independently, could improve plasma production performance.<sup>13</sup> This led to an optimal configuration as in Figure 3a. With this magnetic profile, the discharge runs best with  $\omega_{RF} \simeq \omega_{LH}$  under the antenna. Typical output profiles, density and Mach number, for this configuration are presented in Figure 7.

More recently, by flipping the helicon power feed vacuum section top to bottom, we explored shifting the antenna closer to the magnetic mirror. Provided that the quartz tube is long enough downstream of the antenna, we find similar performance with this antenna location as the profiles show in Figure 7. Figure 3b shows the optimized magnetic configuration. In this configuration,



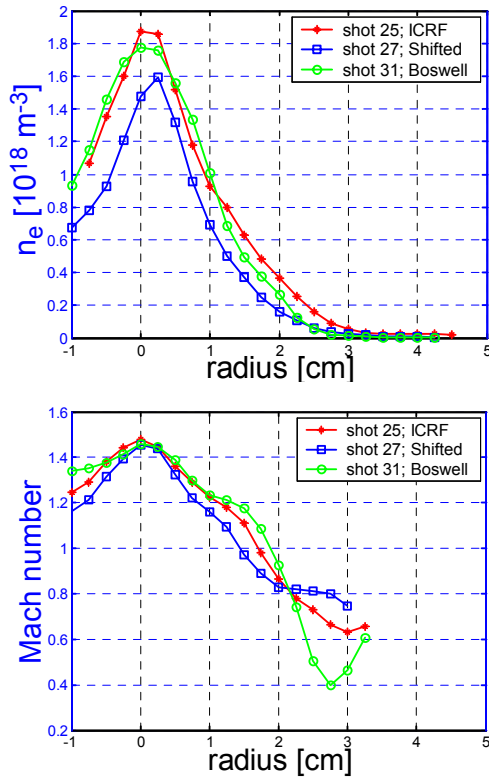


**Figure 7** Electron density and Mach number profiles for three geometries corresponding to Figure 3.

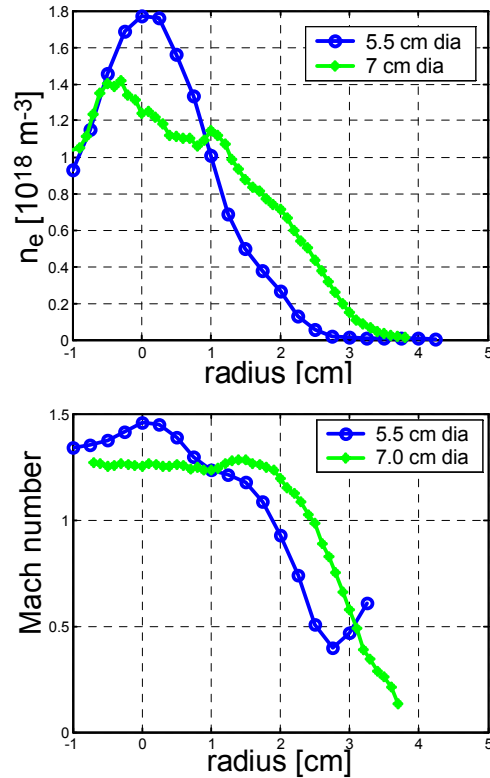


**Figure 8** Profiles comparing the 5.5 cm to the 7 cm diameter helicon with the same input power.

the best performance with helium was with  $\omega_{RF} < \omega_{LH}$  under the antenna, where  $\omega_{RF} = \omega_{LH}$  for deuterium.

Quite recently we converted to a double saddle (Boswell) antenna structure and applied a cusped field configuration upstream of the antenna. Figure 3c shows the optimized magnetic configuration, where  $\omega_{RF} = \omega_{LH}$  under the antenna. The profiles, shown in Figure 7, are very similar to those measured with the previous antenna configurations. Most strikingly, however, we find the optimum gas efficiency with a much lower gas flow rate, by almost a factor of two, 100 sccm versus 200 sccm previously.

We have enlarged the diameter of the Boswell helicon configuration from a 5.5 cm to 7 cm diameter. Figure 8 shows that the profiles broaden and became more flat for the same input power (3 kW) and a doubled input rate. Even though the peak density decreased, the total plasma flux increased by about a factor of 2, approximately proportional to the increased gas input. This indicates a favorable power efficiency scaling with plasma size. The following section characterizes this larger 7 cm diameter discharge by presenting further measurements. The addition of the gas choke has reduced the optimum input gas flow rate by another factor of two.

### **Discharge characteristics**

The magnetic field line that maps back to the quartz tube in the helicon source corresponds well with the plasma edge, indicating little radial transport between the source and exhaust. The electron temperature is nearly constant across the profile, about 6 eV. Visually, there is always a bright core in the discharge.

Figure 4 contains graphs showing temporal behavior during a plasma discharge, without the gas choke. The applied magnetic field is static and a gas pulse is initiated at  $t = 400$  ms. When the

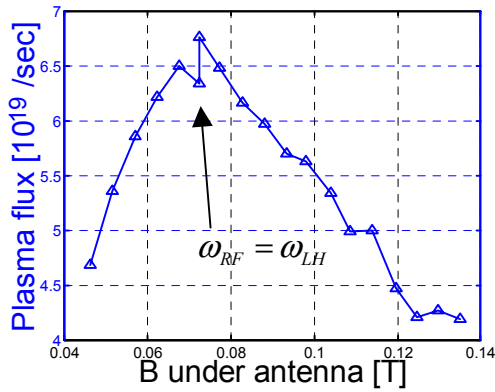


**Figure 9** Plasma flux measured during a scan of the magnetic field under the helicon antenna.

gas flow is established, the RF power is applied. The Mach probe is fixed at two radial locations, center and 2 cm. The ion saturation current on the probe quickly reaches equilibrium, but increases slightly through the discharge. Most interesting is the drop in the Mach number in the first second of the discharge. This is consistent with the plasma exhaust slowing down, due to charge exchange on the increasing background neutral pressure. This effect has also been observed by the RPA.<sup>8</sup> Subsequent Mach probe profiles are acquired in the first 0.5 second of the discharge. Temporal behavior of the neutral pressures are discussed in the next section.

We scanned the magnetic field at the helicon antenna to verify the optimum magnetic field strength there. Figure 9 contains the plasma flux measured for that scan. Clearly the maximum plasma flux measured downstream is with  $\omega_{RF} = \omega_{LH}$  at the helicon antenna.

The ion flux accounts for a large fraction of the incoming gas flow. We plot in Figure 10 the plasma flux measured while scanning the input gas flow for 1, 2, 2.5 and 3 kW power levels. We find a broad range of gas flow,  $\Gamma_{gas} = 2 - 4 \times 10^{19} \text{ sec}^{-1}$ , where  $\eta_{gas} \approx 1$ . Figure 11 shows  $\langle T_e \rangle$  for the flow scan with input power of 3 kW. We see that the temperature rises substantially at the lower flow rate, which is further evidence for a high degree of ionization. The RPA configured as an electron diagnostic also confirms the rise in  $T_e$ .

### **Neutral Dynamics**

We have observed a strong coupling between the plasma discharge and neutral pressure measured inside the quartz tube. Figure 8 includes the temporal behavior of the neutral pressure during a pulsed discharge. When the discharge forms, the pressure rises by almost a factor of four, indicating the importance of charge exchange collisions in establishing the neutral flow. We also observe that this neutral pressure correlates with the plasma flux measurements downstream.<sup>13</sup> The chamber pressure shows a drop with plasma in the exhaust region. This reflects that a significant flux of plasma, comparable to the neutral flux, is flowing through this region.

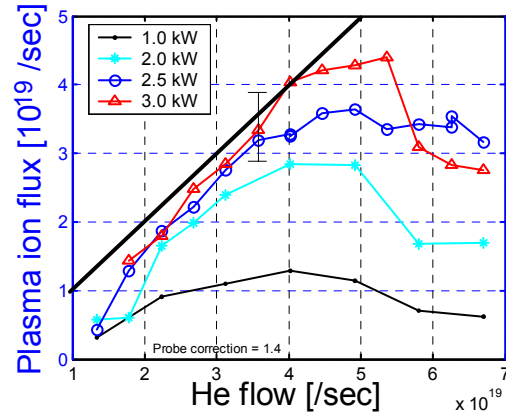


**Figure 10** Plasma flux for 4 power levels with a scan of the input gas number rate.  $\eta_{gas} = 1$  is also plotted.

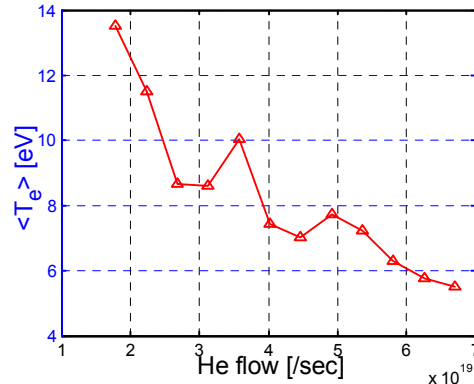


**Figure 11** Profile averaged electron temperature during a scan of the input gas flow, 3 kW RF power.

There is a strong modification in the neutral pressure axial profile with a discharge present, as Figure 12 shows. With no plasma the pressure varies linearly along the quartz tube as expected. A steep gradient in pressure is measured just upstream of the antenna, which is likely balanced by the plasma discharge forming there as indicated by the light emission, also plotted for reference.

### Axial profile measurements

Axial profiles of visible light emission intensity and quartz tube heating from the helicon discharge are shown in Figures 13 and 14 for both helium and deuterium. Light emission and heating are both maximum near the helicon antenna. The light emission profiles for helium and deuterium are strikingly similar. The emission drops rapidly upstream of the antenna at an axial location corresponding to the magnetic cusp. Note that the heating in the helium case is much more localized, which may be attributed to the higher excitation potential of He as compared to D. Surprisingly, the integrated values of the heating profiles are almost the same for the two gases. The input power (3 kW) is the same and the input number rate of atoms is nearly the same ( $\sim 8 \times 10^{19} \text{ sec}^{-1}$ ).

### ICRF

A self-consistent nonlinear theory has been developed predicting ICRF acceleration of ions in the VX-10 type magnetic configuration.<sup>14</sup> Waves are excited on the high magnetic field side of an ion cyclotron resonance,  $\omega_{RF} = \omega_{ci}$ , and they propagate downstream to the resonance where the wave energy is transferred to motion of the ions, with a single pass through the resonance.

Experiments have been performed at the ASPL in which 3 kW of power at 3 MHz was applied to the simple ICRF antenna array. The ion cyclotron resonance was placed just downstream of the antenna array. The magnetic field profile used was like that in Figure 3a, except the peak magnetic field was doubled. Due to the large magnetic field ratio from the helicon to the ICRF section, the plasma size at the ICRF antenna was small, which gave rise to weak coupling between the antenna and plasma. Therefore, in this initial configuration, we did not expect large effects on the plasma

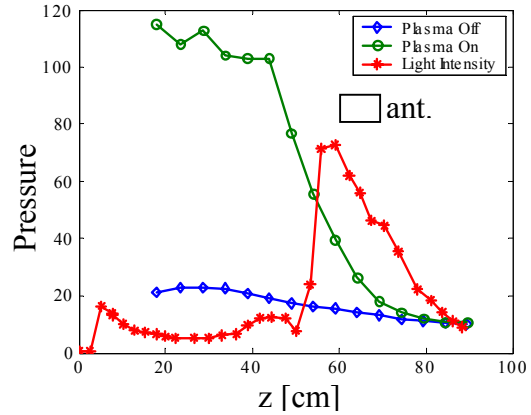


**Figure 12** Axial profile measurement of the neutral pressure inside of the quartz tube. Light emission plotted for reference.

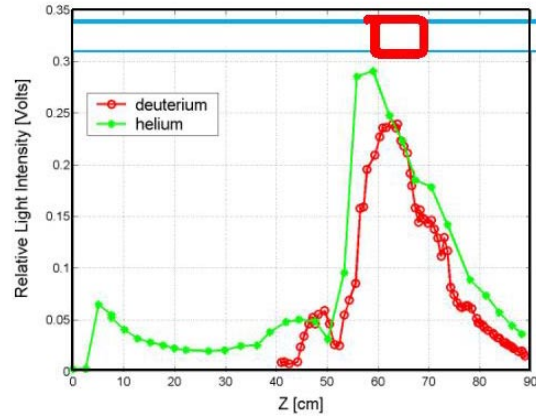


**Figure 13** Axial profile measurement of the visible light emission for both helium and deuterium discharges.

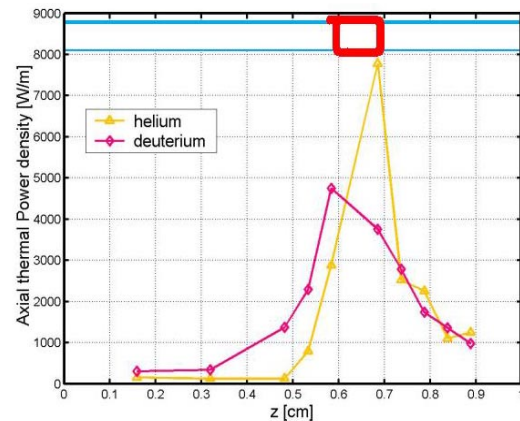


**Figure 14** Axial profile of heating of the quartz tube for both helium and deuterium discharges.



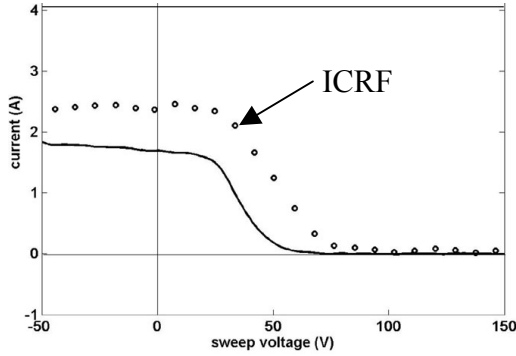


**Figure 15** Right-hand polarized power applied to the ICRF antenna causes the collimated RPA current to increase.

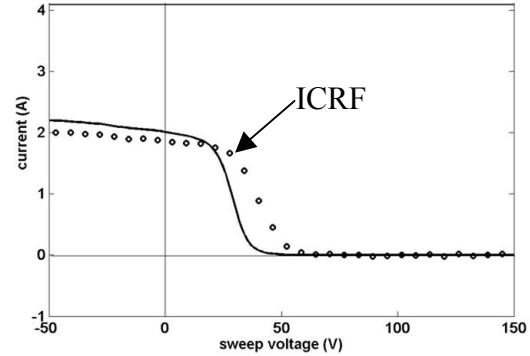


**Figure 16** Left-hand polarized power applied to the ICRF antenna causes the collimated RPA current to decrease.

discharge with the application of ICRF power. Nevertheless, the collimated RPA shows tantalizing data.

RPA data with the collimator were taken with and without the application of ICRF power. Additionally, we tested the effect of reversing the RF phasing on the antenna array. Figure 15 illustrates the effect on the RPA characteristic with the antenna phased in the right-hand (RH) sense or  $m = +1$ . We expect stronger coupling to the electrons in this polarization, with little power coupled directly to ions. The ion current and energy both rise in the RPA, which is consistent with an increase in plasma potential that leads to higher collimator transmission. The probes do not show a large plasma density rise.

In contrast, when the array is polarized in the left-hand (LH) sense or  $m = -1$ , we expect some direct coupling of the power to the perpendicular energy of the ions. This is exhibited in Figure 16 by an ion current drop in the RPA. The ion energy also rises, but this is likely mostly due to plasma potential modification by the high RF fields.

Recent experiments have also been carried out with the second ion cyclotron harmonic,  $\omega_{RF} = 2\omega_{ci}$ . Results from these experiments have been reported in another paper.<sup>13</sup>

## FUTURE

We are in the process of enlarging the helicon source diameter to 9 cm with a gas choke incorporated. An RF drive frequency of 50 MHz will soon be explored, which we expect will double the optimal magnetic field for the helicon and increase the plasma size at the ICRF antenna location. Additionally, we are doubling the power available for the helicon source. The upgraded plasma target will increase the plasma loading for the ICRF and make application of larger amounts of power possible. With this upgrade, we will return to ICRF experiments early this year. Extensive ICRF antenna design work has begun.

## CONCLUSION

We have described the VASIMR experiment (VX-10) that is being performed at the Advanced Space Propulsion Laboratory (ASPL) of NASA's Johnson Space Center. Recent work with the helicon plasma source has produced a potentially more compact and efficient design. This design has achieved near 100% gas utilization. Key features of the latest design is a double saddle (Boswell) antenna, a magnetic cusp applied upstream of the antenna and a gas choke downstream at the magnetic maximum. Most recently we have enlarged the diameter of the helicon source with positive effects that indicate favorable scaling with size. There is a strong coupling between the plasma and neutrals in the source. Axial measurements of neutral pressure, visible light

emission, and quartz tube heating in the helicon indicate localized plasma production near or under the helicon antenna.

Ion Cyclotron Resonance Frequency (ICRF) experiments have shown tantalizing effects with the resonance located just downstream of the antenna array. A highly collimated Retarding Potential Analyzer (RPA) shows evidence of perpendicular heating of ions as predicted. Upgrades that are in progress with the helicon plasma source will significantly increase the measurable effects with ICRF. We expect more substantial results in the very near future.

### NOMENCLATURE

$C_s$	ion sound speed	$\eta_{gas}$	gas efficiency
$I_{sat}$	probe ion saturation current	$\omega_{LH}$	lower hybrid frequency
$M$	plasma Mach number	$\omega_{ce}$	electron cyclotron frequency
$m_i$	ion mass	$\omega_{ci}$	ion cyclotron frequency
$n_e$	electron density	$\omega_{pi}$	ion plasma frequency
$T_e$	electron temperature	$\omega_{RF}$	radio frequency drive frequency
$\Gamma_{plasma}$	total plasma flux		
$\Gamma_{gas}$	input gas number rate		

### ACKNOWLEDGMENTS

This research was sponsored by NASA Johnson Space Center. The authors would like to recognize the valuable contributions of Garland W. Goebel, Greg E. McCaskill and D. Scott Winter.

### REFERENCES

1. F. R. Chang Diaz, "An Overview of the VASIMR Engine: High Power Space Propulsion with RF Plasma Generation and Heating", RADIO FREQUENCY POWER IN PLASMAS : 14<sup>th</sup> Topical Conference, Oxnard, CA, *AIP Conference Proceedings* **595**, 3 (2001).
2. R. W. Boswell and F. F. Chen, Helicons, the Early Years, *IEEE. Transactions of Plasma Science*, **25**, 1229-1244, (1997).
3. F. F. Chen and R.W. Boswell, Helicons, The Past Decade, *IEEE. Transactions of Plasma Science*, **6**, 1245-1257, (1997).
4. J. P. Squire, F. R. Chang Díaz, V. T. Jacobson, G. E. McCaskill, R. D. Bengtson, R. H., Goulding, "Helicon Plasma Injector and Ion Cyclotron Acceleration Development in the VASIMR Experiment", *Proceedings of 36<sup>th</sup> AIAA/ASME/SAE/ASEE Joint Propulsion Conference (Huntsville, Alabama 2000)* AIAA 2000-3752.
5. Hutchinson, I.H., *Phys. Rev. A*, **37**, 4358 (1987)
6. P. C. Stangeby, *Phys. Fluids*, **27**, 2699 (1984)
7. D.G. Chavers, F. R. Chang Díaz, and J. P. Squire, "MOMENTUM AND HEAT FLUX MEASUREMENTS IN THE EXHAUST OF VASIMR USING HELIUM PROPELLANT", this conference.
8. T. G. Glover, "Measurement of Plasma Parameters in the Exhaust of a Magnetoplasma Rocket by Gridded Energy Analyzers and Emissive Langmuir Probe", Ph.D. thesis, Rice University (2002).
9. P. Zhu and R. W. Boswell, *Phys. Rev. Lett.* **63**, 2805 (1989).
10. S.-M. Yun, J.-H. Kim, and H.-Y. Chang, *J. Vac. Sci. Technol. A* **15**, 673 (1997).
11. M. D. Carter, et al., "Comparing Experiments with Modeling for Light Ion Helicon Plasma Sources", accepted for publication in *Phys. Plasmas*.
12. Stix, T. *Waves in Plasmas* (American Institute of Physics, New York, 1992).
13. J. P. Squire, F. R. Chang Díaz, T. W. Glover, V. T. Jacobson, D. G. Chavers, R. D. Bengtson, E. A. Bering, III, R. W. Boswell, R. H. Goulding and M. Light, "Progress in Experimental Research of the VASIMR Engine" *TRANSACTIONS of Fusion Science and Technology*, to be published late 2002.
14. B. N. Breizman and A. V. Arefiev, *Phys. Plasmas* **8**, 907 (2001).